nature photonics

Article

https://doi.org/10.1038/s41566-023-01212-1

Demonstration of the quantum principle of least action with single photons

Received: 24 October 2021

Accepted: 18 April 2023

Published online: 22 May 2023

Check for updates

Yong-Li Wen[1,2,3,4], Yunfei Wang[1,2,4], Li-Man Tian[1,2,4], Shanchao Zhang[1,2], Jianfeng Li[1,2], Jing-Song Du[1,2], Hui Yan[1,2] ✉ & Shi-Liang Zhu[1,2] ✉

The principle of least action is arguably the most fundamental principle in physics as it can be used to derive the equations of motion in various branches of physics. However, this principle has not been experimentally demonstrated at the quantum level because the propagators for Feynman's path integrals have never been observed. The propagator is a fundamental concept and contains various significant properties of a quantum system in the path integral formulation, so its experimental observation is itself essential in quantum mechanics. Here we theoretically propose and experimentally observe the propagators of single photons based on the method of directly measuring quantum wave functions. Furthermore, we obtain the classical trajectories of single photons in free space and in a harmonic trap based on the extremum of the observed propagators, thereby experimentally demonstrating the quantum principle of least action. Our work paves the way for experimentally exploring the fundamental problems of quantum theory in the formulation of path integrals.

The principle of least action (PLA) is a variational principle that—when applied to the action of a mechanical system—can be used to obtain the equations of motion for that system. The PLA is possibly the most fundamental principle in physics because the fundamental laws in various branches of physics, such as classical mechanics, electrodynamics, special and general relativity, quantum mechanics and quantum field theory, can be derived from the PLA[1–3]. Historically, the PLA has been used in several different contexts, such as Hamilton's principle and Maupertuis' principle in classical mechanics, as well as Fermat's principle of least time in optics. Intriguingly, although Einstein did not follow a least action approach in his theories of relativity, Planck formulated the dynamics of special relativity using the PLA in 1907. More interestingly, after Hilbert learned about Einstein's initial idea of general relativity, he followed the PLA approach, guessed the 'most natural' Lagrangian in 1915 and derived the gravitational field equations before Einstein[1]. By extending the PLA to quantum mechanics, Feynman discovered the path integral formulation of quantum mechanics, which is a crucial representation of quantum mechanics and has profoundly advanced the development of theoretical physics[2,3].

For non-quantum systems, an experimental demonstration of the PLA is easy since the trajectory of the system can be readily observed. However, this principle has not been experimentally demonstrated at the quantum level because of two obstacles. One is a conceptual obstacle, and the other is a technical one. Conceptually, one can determine the unique trajectory of a classical object moving from an initial position to a final position, but in quantum mechanics, according to Heisenberg's uncertainty principle, position and momentum cannot be simultaneously measured. Furthermore, any path connected with initial and final points is possible in quantum mechanics, so a unique trajectory like that in non-quantum physics does not exist. Feynman's path integral formulation creates a bridge between the classical Lagrangian description of the physical world and the quantum one, reintroducing the classical concept of trajectory to quantum mechanics. Technically, the PLA in Feynman's path integrals is associated with a core quantity called propagator, which has never been experimentally observed.

[1]Guangdong Provincial Key Laboratory of Quantum Engineering and Quantum Materials, School of Physics and Telecommunication Engineering, South China Normal University, Guangzhou, China. [2]Guangdong-Hong Kong Joint Laboratory of Quantum Matter, Frontier Research Institute for Physics, South China Normal University, Guangzhou, China. [3]National Laboratory of Solid State Microstructures and School of Physics, Nanjing University, Nanjing, China. [4]These authors contributed equally: Yong-Li Wen, Yunfei Wang, Li-Man Tian. ✉e-mail: yanhui@scnu.edu.cn; slzhu@scnu.edu.cn

https://doi.org/10.1038/s41566-023-01212-1

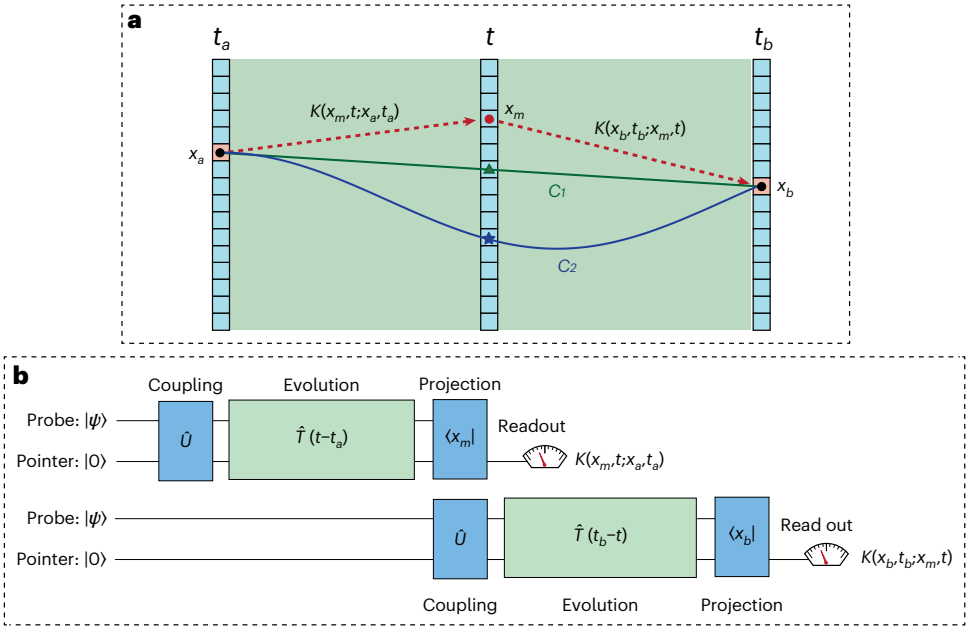

Fig. 1 | Schematic of path integrals and measuring method. a, Propagators and classical trajectories. C_1 (C_2) is the classical trajectory in free space (harmonic potential). The propagation from (x_a, t_a) to (x_b, t_b) is divided into two parts with intermediate points (x, t). The product of propagators $K(x_b, t_b; x, t)K(x, t; x_a, t_a)$ is used to determine the classical trajectory. The classical position in free space (harmonic potential) determined by equation (2) is shown as the green triangle (blue star). **b**, Protocol to measure the propagators. For the measurement of $K(x_m, t; x_a, t_a)$, the quantum state $|\psi\rangle$ and pointer $|0\rangle$ are prepared. Then, at time t_a, a coupling operation $\hat{U}$ allows the probe system to shift the pointer at position x_a. After the evolution, the system is projected to position x_m at t, and $K(x_m, t; x_a, t_a)$ can be read from the pointer. Similarly, $K(x_b, t_b; x_m, t)$ can be measured by performing $\hat{U}$ at t and projecting the system to x_b at t_b.

This propagator is a complex amplitude with both real and imaginary components and thus cannot be measured by conventional projective measurement schemes. Recently, a method known as 'direct measurement' was developed[4] to measure the quantum wave functions[5–12]. With this method, the real and imaginary components of the quantum wave function can be directly read from the measuring equipment based on an interesting concept called weak value[13–15]. The weak value has been widely used in precision metrology[16–18] and the observation of non-classical paths[19–22].

In this Article, we report the first experiment to measure the propagators of single photons in Feynman's path integrals and then demonstrate the PLA at the quantum level. We theoretically develop a 'direct measurement' method to observe the propagators (in the sense of directly reading them from the experimental apparatus) and then experimentally adopt this approach to measure the real and imaginary components of the propagators. Furthermore, by analysing the extremum of the measured propagators, we experimentally demonstrate the PLA in Feynman's path integrals with single photons.

Results

Theoretical model

Figure 1a reviews some basic concepts of path integrals. We assume an initial wave function $|\psi(x_a, t_a)\rangle$ at a fixed position x_a and time t_a and use them to determine the wave function $|\psi(x_b, t_b)\rangle$ at another fixed position x_b and time t_b. Here $|\psi(x_b, t_b)\rangle = K(x_b, t_b; x_a, t_a)|\psi(x_a, t_a)\rangle$ in the path integral formulation, where the propagator $K(x_b, t_b; x_a, t_a)$ describes the transition from the initial state $|\psi(x_a, t_a)\rangle$ to the final state $|\psi(x_b, t_b)\rangle$. Given an arbitrary position x at intermediate time t, the propagator $K(x_b, t_b; x_a, t_a)$ can be obtained by the integration

$$K(x_b, t_b; x_a, t_a) = \int \Pi(x, t)\mathrm{d}x = \mathcal{N}\mathrm{e}^{(\mathrm{i}/\hbar)S_{\mathrm{cl}}}, \quad (1)$$

where $\Pi(x, t) \equiv K(x_b, t_b; x, t)K(x, t; x_a, t_a)$, S_{cl} is the classical action of the path and $\mathcal{N}$ is a normalization constant. The classical trajectory complies with the PLA and satisfies the variational equation of $\delta S/\delta x(t) = 0$, where S is the action. When the ratio of action S to the Planck constant $\hbar$ increases, the phase factor $\mathrm{e}^{(\mathrm{i}/\hbar)S}$ behaves as a strong oscillatory function, and according to a heuristic extrapolation of the stationary phase method to the path integral case, the main contribution should come from those paths that make the phase function stationary. Therefore, one can derive a classical-like trajectory of the system from the PLA.

The variational formulation of the PLA is difficult to demonstrate in experiments; however, for fixed initial and final positions x_a and x_b, the stationary of action S leads to

$$\frac{\partial}{\partial x}\Pi(x, t) = 0 \quad (2)$$

for any time t, so the classical trajectory at intermediate position x should satisfy equation (2), and this form of the PLA can be readily demonstrated in experiments. The analytical expressions of the propagators for a particle in free space and in harmonic potential are provided in Methods. Substituting these expressions in equation (2), we obtain that the classical trajectory is a straight line (cosine type of curve) for a particle moving from (x_a, t_a) to (x_b, t_b) in free space (harmonic potential) (Fig. 1a). Therefore, by changing the intermediate time t, the classical trajectory connecting two points can be derived with equation (2), and the PLA at the quantum level can be demonstrated if the propagators are measured.

We now describe our approach to measure the propagators of single photons and to demonstrate the PLA. The schematic of this method is shown in Fig. 1. For simplicity, we assume that the photons propagate along the z direction and that the initial wave function is a Gaussian wave packet so we can focus on the x–z plane. As shown in Methods, the system we studied can be considered as a one-dimensional system with x as the position coordinate and z as the propagation time with

https://doi.org/10.1038/s41566-023-01212-1

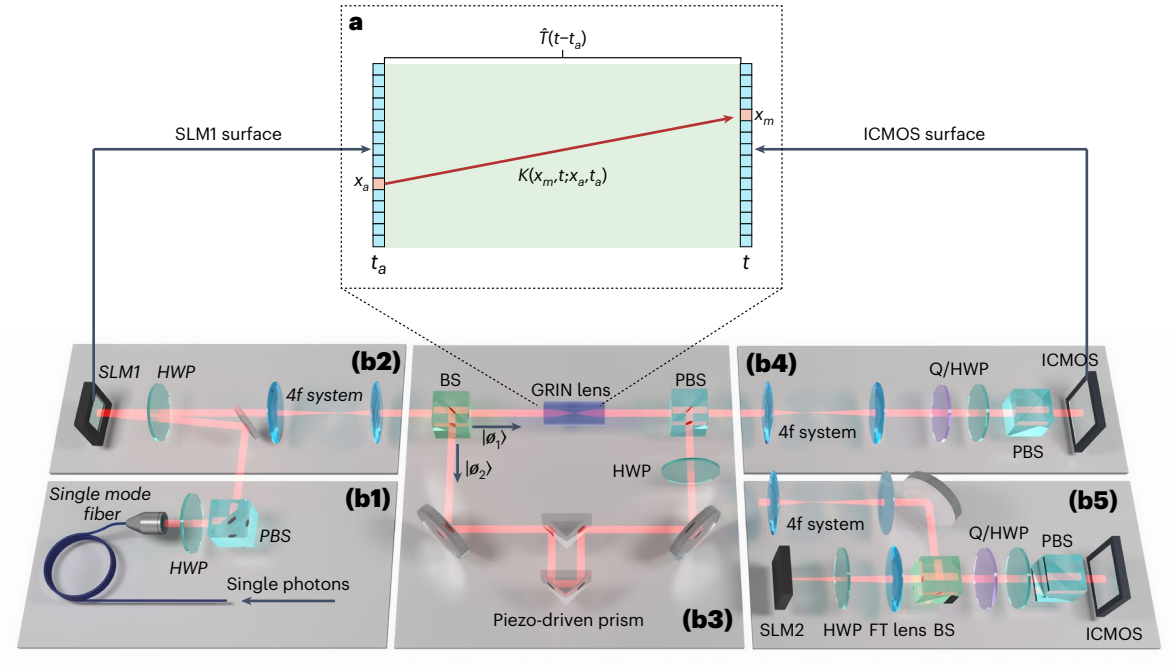

Fig. 2 | Schematic of the experiment. a, Evolution and detection region. For the measurement of $K(x_m, t; x_a, t_a)$, a SLM1 accomplishes coupling $\hat{U}$ at position x_a, whereas the ICMOS camera measures the photon spatial distribution at all positions x for $z = ct$. **b**, Experimental setup. State initialization (i): single photons with a Gaussian transverse mode emerge from a single-mode fibre and are initialized to the vertical polarization state $|0\rangle$. Spatial-pointer coupling (ii): the combination of HWP, SLM1 and 4*f* system realizes the $\hat{U}$ operation only at assigned positions, such as x_a. State evolution (iii): the photons are split into two branches $|\phi_1\rangle$ and $|\phi_2\rangle$ by a 50:50 beamsplitter (50:50 BS). The $|\phi_1\rangle$ branch is sent into the region with Hamiltonian H corresponding to the measured propagator $K(x_m, t; x_a, t_a)$. A GRIN lens produces a harmonic potential, and the absence of the GRIN lens implies free propagation. After the evolution, these two branches are merged by a PBS. The piezo-driven prism is used to stabilize the optical path difference between these two branches. Post-selection of position and readout of the pointer (iv): a 4*f* system transits the wavefront at the measured positions ($z = ct$ or $z = ct_b$) to the ICMOS camera. Each detection of photons on the ICMOS camera is gated[26] (Supplementary Section 2). Different image planes of t can be measured by adjusting the longitudinal position of the ICMOS camera. The QWP or HWP and the PBS between the 4*f* system and ICMOS camera are used to read the expectations of the pointer. Measurement of wave function (v): a combination of an Fourier transform (FT) lens, an HWP and an SLM (HOLOEYE, PLUTO-2-NIR-011) accomplishes a coupling between the transverse momentum and the polarization of photons. The ICMOS camera measures the spatial distribution of the photons of the five bases of polarization, namely, $\{|+\rangle, |-\rangle, |R\rangle, |L\rangle, |1\rangle\}$.

$t = z/c$ (c is the velocity of light). We use the propagator $K(x, t; x_a, t_a)$ as an example to describe our measurement method.

We take the spatial mode as the explored system and the polarization of photons as the pointer. The initial state is $|\psi\rangle|0\rangle$, where $|0\rangle$ is the pointer state. At initial moment t_a, we use a coupling operation $\hat{U} = e^{-i\frac{\pi}{2}\hat{\pi}_{x_a}\hat{\sigma}_y}$ to couple the spatial mode of the single photons to the pointer. Here, $\hat{\pi}_x = |x\rangle\langle x|$ and $\hat{\sigma}_{x,y,z}$ are Pauli matrices acting on the pointer states. This coupling only allows the photons at position x_a shifting the pointer. Then, the photons enter the region with potential $V(x)$ for the evolution $\hat{T}(t - t_a) = \exp(-\frac{i}{\hbar}\int_{t_a}^{t} H dt')$ governed by the Hamiltonian $H = p_x^2/2m + V(x)$. In our experiment, we choose either free space or harmonic potential for this evolution. We terminate the evolution by measuring the pointer state at position x_m and time $t = z/c$. In Methods, we show that the propagator $K(x_m, t; x_a, t_a)$ can be obtained by

$$K(x_m, t; x_a, t_a) = \frac{K''(x_m, t; x_a, t_a)}{\sqrt{2}\psi^*(x_m, t_a)\psi(x_a, t_a)}, \quad (3)$$

where $K''(x_m, t; x_a, t_a) = -\langle f|\hat{\sigma}_x|f\rangle + i\langle f|\hat{\sigma}_y|f\rangle$ and $|f\rangle$ denote the final state of the pointer. Also, $\psi^*(x_m, t_a)$ and $\psi(x_a, t_a)$ are the spatial wave functions of the photons, which can be measured by the 'direct measurement' method[4,9]. Scanning the projecting position x_m allows us to measure $K(x, t; x_a, t_a)$ as a function of x. Similarly, we can derive the propagator $K(x_b, t_b; x, t)$ by scanning the coupling position x_m at moment t and the projection position x_b is fixed. With the measured $K(x, t; x_a, t_a)$ and $K(x_b, t_b; x, t)$ as a function of x, we use equation (2) based on the PLA to analyse the extremum of the product $\Pi(x, t) = K(x_b, t_b; x, t)K(x, t; x_a, t_a)$ and to derive the classical trajectories of single photons.

Experimental measurement of propagators

We perform an experiment to measure the propagators $K(x, t; x_a, t_a)$ and $K(x_b, t_b; x, t)$ of single photons. The schematic of our experiment is shown in Fig. 2. In our experiment, single photons are produced through spontaneous parametric downconversion[23–25], with the second-order correlation function $g_c^{(2)} = 0.094 \pm 0.011$ and a centre wavelength of $\lambda = 795$ nm (Supplementary Section 2 and refs. 26–29).

We use a half-wave plate (HWP) and a spatial light modulator (SLM1; HOLOEYE, PLUTO-2-NIR-080) to couple the transverse spatial wave function to the pointer. The SLM1 rotates the polarization of photons by π/2 only at position x_a. This modulation corresponds to the unitary evolution $\hat{U} = e^{-i\frac{\pi}{2}\hat{\pi}_{x_a}\hat{\sigma}_y}$. We assume that the moment right after the modulation on SLM1 is t_a. The modulated photons then enter a 4*f* system and are split into two paths. One of these paths passes through the region with an evolution $\hat{T}(t - t_a)$, and the other path is virtually stationary. The 4*f* system transits the spatial mode of the photons from the surface of SLM1 to the evolution area. As shown in Fig. 2b, the spatial-pointer coupling takes place at moment t_a. In the evolution area, the effective potential $V(x)$ is proportional to the refractive index. Thus, we use a material with a quadric refractive-index distribution to realize

https://doi.org/10.1038/s41566-023-01212-1

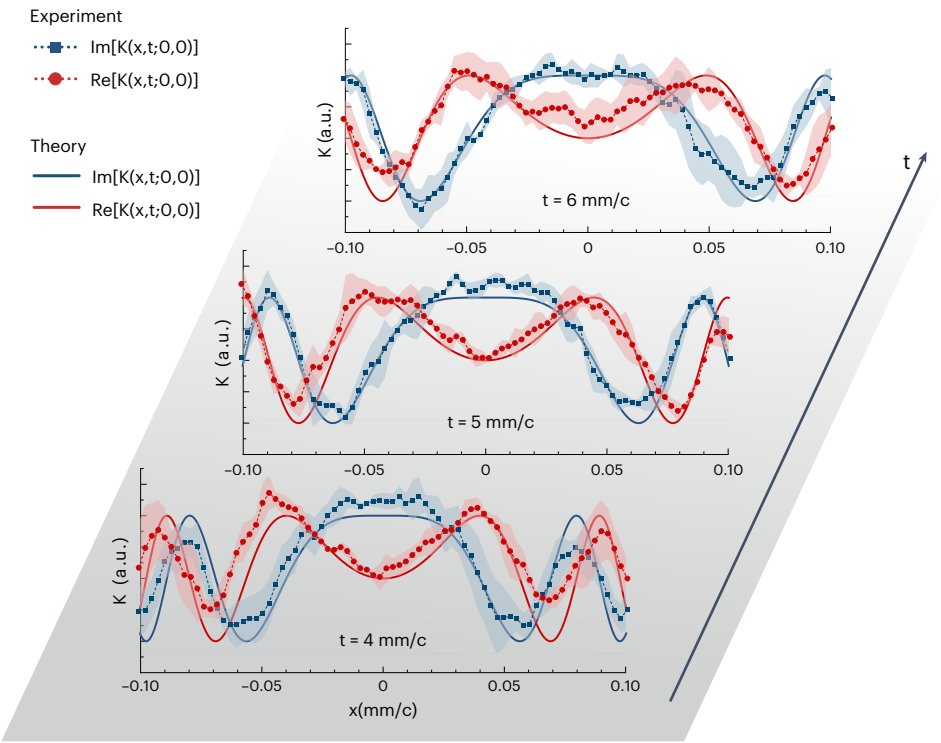

Fig. 3 | Measured propagators of single photons in free space. The propagators $K(x, t; 0, 0)$ with arbitrary unit (a.u.) as a function of x at $t = \{4\ \text{mm}\ c^{-1}, 5\ \text{mm}\ c^{-1}, 6\ \text{mm}\ c^{-1}\}$. The solid lines are theoretical results of the real (red) and imaginary (blue) propagators. The red circles (blue squares) and shaded error bands represent the mean value and standard deviation of three repetitive measurements.

a harmonic potential for single photons and use air with a uniform refractive index to achieve free space. Another 4f system transits the spatial mode at t to an intensified complementary metal–oxide–semiconductor (ICMOS) camera (CISS, 2DSPC; quantum efficiency, 32%; pixel size, 9 μm; readout noise, 4.68 e^- per pixel per second). This operation realizes the projection of x, since the ICMOS camera can measure the spatial distribution of photons. The positions of the pixels on the camera indicate the projecting position. Before the photons are collected by the ICMOS camera, we select the polarization with four bases: two diagonal polarization bases ($|+\rangle$ and $|-\rangle$) and two circular polarization bases ($|R\rangle$ and $|L\rangle$). The readouts from the camera on these four bases are used to calculate the expectation values in equation (3).

We place a gradient refractive index (GRIN) lens at the path of $|\phi_1\rangle$, where the incident surface of the GRIN lens is at the image plane of the 4f system (Methods). Therefore, the GRIN lens carries out the evolution $\hat{T}_1(t_b - t_a)$, where t_a (t_b) is the incident (exit) surface. For the free-propagation case, the GRIN lens is removed. The outgoing photons from this evolution then pass through a polarizing beamsplitter (PBS). This PBS projects $|\phi_1\rangle$ to pointer state $|1\rangle$ by selecting the transmitted photons. For the other branch $|\phi_2\rangle$, we add an HWP before the PBS, and the reflected photons are projected to state $|-\rangle$. The PBS merges these two branches into one. The second 4f system is placed after the PBS transits the state from the t_b plane to the ICMOS camera. The camera is used to measure the spatial distribution of the photons. The intensity of the pixel at position x_b on the ICMOS sensor represents the readout of post-selection $|x_b\rangle$. To read the expectation values of $\langle f|\hat{\sigma}_y|f\rangle$ and $\langle f|\hat{\sigma}_x|f\rangle$, we set a quarter-wave plate (QWP) or HWP and a PBS to project the photons onto the following four polarization bases: $|+\rangle = 1/\sqrt{2}(|0\rangle + |1\rangle)$, $|+\rangle = 1/\sqrt{2}(|0\rangle - |1\rangle)$, $|R\rangle = 1/\sqrt{2}(|0\rangle + \mathrm{i}\,|1\rangle)$ and $|L\rangle = 1/\sqrt{2}(|0\rangle - \mathrm{i}\,|1\rangle)$. The intensities of the pixels on these four bases are $\{P_+, P_-, P_R, P_L\}$, respectively. The difference between P_+ and P_- gives the expectation of $\langle f|\hat{\sigma}_x|f\rangle = P_+ - P_-$, whereas the difference between P_R and P_L gives the expectation of $\langle f|\hat{\sigma}_y|f\rangle = P_R - P_L$.

To measure the wave functions $\psi(x_a, t_a)$ and $\psi(x_m, t_a)$, we perform an interaction $\hat{U}_p = \mathrm{e}^{-\mathrm{i}\frac{\pi}{2}\hat{\pi}_{p_0}\hat{\sigma}_y}$ to couple the momentum of the photons to the pointer and then use the ICMOS camera to project the system to the position state $\langle x_j|$ (Fig. 2b(v) and Supplementary Section 1)[26]. Similarly, using a QWP/HWP and a PBS to read the expectation values of $\hat{\sigma}_y$, $\hat{\sigma}_x$ and $\hat{P}_1 = |1\rangle\langle 1|$, we have

$$\psi(x_j, t_a) = -\frac{\frac{1}{2}[\langle f_j|\hat{\sigma}_x|f_j\rangle + \mathrm{i}\langle f_j|\hat{\sigma}_y|f_j\rangle] - \langle f_j|\hat{P}_1|f_j\rangle}{\Phi^*(0, t_a)}, \tag{4}$$

where $j = \{m, a\}$ is the index of the measured position[26] (Supplementary Section 1).

The propagators of single photons in free space are shown in Fig. 3. We choose $x_a = 0$ as a fixed initial point and then measured the propagators $K(x, t; x_a, t_a)$ as a function of final position x. By adjusting the ICMOS camera on the longitudinal axis, we can detect $K(x, t; x_a, t_a)$ at different evolution times t. The experimental results of $K(x, t; x_a, t_a)$ as a function of x and t are shown in Fig. 3 at $t = \{4\ \text{mm}\ c^{-1}, 5\ \text{mm}\ c^{-1}, 6\ \text{mm}\ c^{-1}\}$ with the measuring step $\delta x \approx 2.67$ μm. The experimental data agree well with the theoretical results.

Demonstration of PLA

In Methods, we show that the classical trajectories based on the PLA can be determined by

$$\frac{\partial}{\partial x}\mathrm{Re}[\mathcal{M}''(x, t)] = 0, \quad \frac{\partial}{\partial x}\mathrm{Im}[\mathcal{M}''(x, t)] = 0, \tag{5}$$

where $\mathcal{M}''(x, t) = \Pi''(x, t)/|\Pi''(x, t)|$ with $\Pi''(x, t) = K''(x_b, t_b; x, t)K''(x, t; x_a, t_a)$. Using the same method described in the previous section, we measure both $K''(x, t; x_a, t_a)$ and $K''(x_b, t_b; x, t)$, and the classical trajectory $x_{cl}(t)$ can be obtained by equation (5) with the measured data.

https://doi.org/10.1038/s41566-023-01212-1

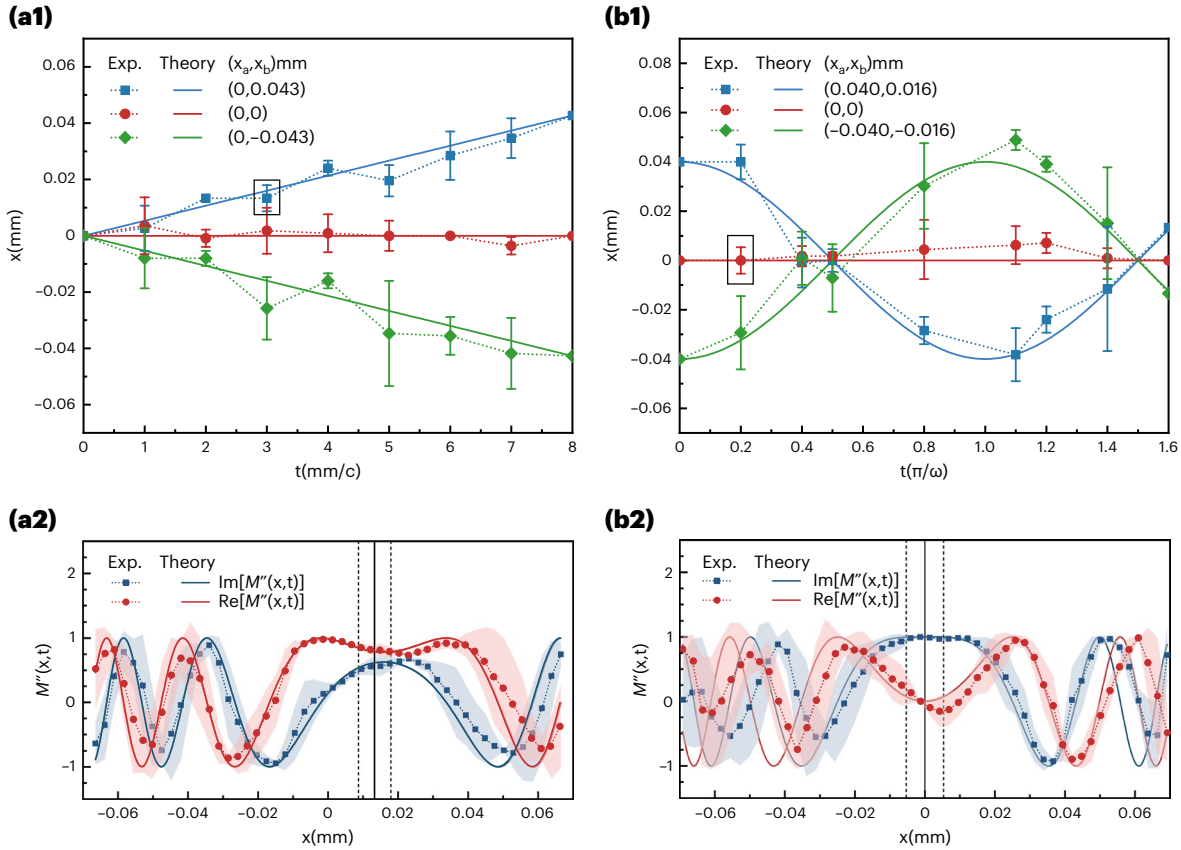

Fig. 4 | Classical trajectories of single photons determined by the PLA. a, Classical trajectories in free space with fixed initial position $x_a = 0$ and three final positions $x_b = \{0.043\ \text{mm}, 0, -0.043\ \text{mm}\}$ (i). **b**, Classical trajectories in the harmonic potential with initial position x_a and final position x_b: $(x_a, x_b) = (0.040\ \text{mm}, 0.016\ \text{mm})$, $(0, 0)$ and $(-0.040\ \text{mm}, -0.016\ \text{mm})$. The solid lines are theoretical results calculated from the analytical expressions (exp.) of the propagators, and the dots with the error bar present the mean value and standard derivation of three repetitive measurements. $\mathcal{M}''(x)$ for the data in frames in **a(i)** and **b(i)** are shown in **a(ii)** and **b(ii)**, respectively. The solid lines are real (red) and imaginary (blue) components of the theoretical results of $\mathcal{M}''(x)$ and the dots are the measured results. The vertical solid (dashed) lines in **a(ii)** and **b(ii)** show the mean value (standard derivation) of the classical positions determined by the measured $\mathcal{M}''(x)$. The dots with the shaded error bands present the mean values and standard deviation of three repetitive measurements.

In the experiments, we select an initial position x_a by choosing the transverse position of the slits on SLM1. Then, $K''(x, t; x_a, t_a)$ as a function of x can be measured by the ICMOS camera. In $K''(x_b, t_b; x, t)$, x is the variable initial position and x_b is the fixed final position. We scan the slits on SLM1 to accomplish the change in x. Also, $K''(x_b, t_b; x, t)$ can be measured by reading the signal of the final position x_b on the ICMOS camera. With these data, we can obtain $x_{cl}(t)$ by searching the position where $\mathcal{M}''(x, t)$ has its extremum. The GRIN lens is used to simulate the harmonic potential, which can be effectively expressed as $V(x) = \frac{1}{2}m\omega^2x^2$(Methods). The GRIN lens is removed when propagators of the free particle are measured.

The classical trajectories determined by the measured propagators are plotted in Fig. 4, where they are a straight line (cosine type of curve) for a particle moving from (x_a, t_a) to (x_b, t_b) in free space (a harmonic potential), as expected by the analytical expressions in equations (8) and (9). The propagators $\mathcal{M}''$ for the data in the dashed frames shown in Fig. 4a(i),b(i) are plotted in Fig. 4a(ii),b(ii), respectively. The classical paths derived from the measured propagators agree well with the theoretical results, whereas the deviation of $\mathcal{M}''$ from the ideal result is small in the region near the classical trajectory but large in the region far away from the classical trajectory. Therefore, the classical trajectories determined by the measured propagators are very robust. This is also true for various perturbations; we use the deviation of time as an example to show this phenomenon (Methods). This phenomenon occurs because the action S is stationary for a classical trajectory but would behave as a strong oscillation function for non-classical trajectories. Our experiment demonstrates this essential idea of the path integral theory[2,3].

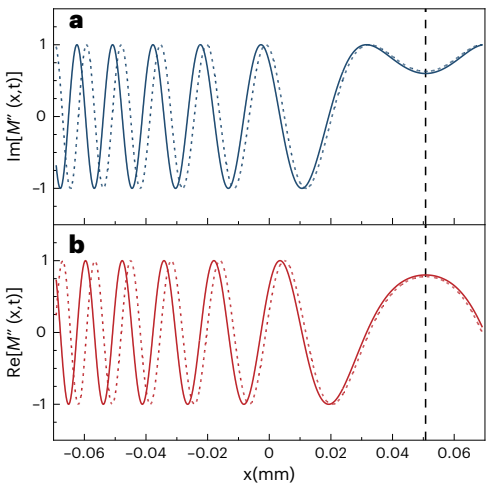

Fig. 5 | Theoretical comparison of $\mathcal{M}''(x, t)$ and $\mathcal{M}''_\epsilon(x, t - \epsilon)$ in the harmonic potential, where $t = 1.1\pi/\omega$ and $\epsilon = 0.003(t_b - t_a)$. a,**b**, Imaginary (**a**) and real (**b**) components of $\mathcal{M}''(x, t)$ (solid) and $\mathcal{M}''_\epsilon(x, t)$ (dashed). The dashed vertical straight line shows the classical position determined by $\mathcal{M}''(x, t)$.

Discussion

In summary, we have reported one of the first experiments to measure the propagators of single photons and to demonstrate the quantum PLA. Feynman's path integral has been recognized as a crucial theory in the development of modern quantum mechanics, particularly in quantum field theory and quantum statistical physics. The propagator, which lies at the heart of this theory, contains significant properties (such as wave function, evolution, action, topological invariants and partition function) of a quantum system. Our method of measuring the propagators provides a new perspective to study quantum systems in the path integral formulation. As our experiment shows, classical trajectories can be obtained by measuring the propagators, which allows us to further explore the crossover between classical physics and quantum physics, one of the frontiers in current physics research. Moreover, the measurement of the propagators opens opportunities for experimentally exploring physics phenomena in quantum field theory and quantum statistical physics that previously could not be experimentally observed.

Online content

Any methods, additional references, Nature Portfolio reporting summaries, source data, extended data, supplementary information, acknowledgements, peer review information; details of author contributions and competing interests; and statements of data and code availability are available at https://doi.org/10.1038/s41566-023-01212-1.

References

1. Rojo, A. & Bloch, A. *The Principle of Least Action: History and Physics* (Cambridge Univ. Press, 2018).
2. Feynman, R. P. Space-time approach to non-relativistic quantum mechanics. *Rev. Mod. Phys.* **20**, 367–387 (1948).
3. Feynman, R. P., Hibbs, A. R. & Styer, D. F. *Quantum Mechanics and Path Integrals* (Dover Publications, 2010).
4. Lundeen, J. S., Sutherland, B., Patel, A., Stewart, C. & Bamber, C. Direct measurement of the quantum wavefunction. *Nature* **474**, 188–191 (2011).
5. Salvail, J. Z. et al. Full characterization of polarization states of light via direct measurement. *Nat. Photon.* **7**, 316–321 (2013).
6. Thekkadath, G. S. et al. Direct measurement of the density matrix of a quantum system. *Phys. Rev. Lett.* **117**, 120401 (2016).
7. Lundeen, J. S. & Bamber, C. Procedure for direct measurement of general quantum states using weak measurement. *Phys. Rev. Lett.* **108**, 070402 (2012).
8. Malik, M. et al. Direct measurement of a 27-dimensional orbital-angular-momentum state vector. *Nat. Commun.* **5**, 3115 (2014).
9. Shi, Z. et al. Scan-free direct measurement of an extremely high-dimensional photonic state. *Optica* **2**, 388–392 (2015).
10. Bolduc, E., Gariepy, G. & Leach, J. Direct measurement of large-scale quantum states via expectation values of non-Hermitian matrices. *Nat. Commun.* **7**, 10439 (2016).
11. Vallone, G. & Dequal, D. Strong measurements give a better direct measurement of the quantum wave function. *Phys. Rev. Lett.* **116**, 040502 (2016).
12. Zhang, S. et al. δ-quench measurement of a pure quantum-state wave function. *Phys. Rev. Lett.* **123**, 190402 (2019).
13. Aharonov, Y., Albert, D. Z. & Vaidman, L. How the result of a measurement of a component of the spin of a spin-1/2 particle can turn out to be 100. *Phys. Rev. Lett.* **60**, 1351–1354 (1988).
14. Ritchie, N. W. M., Story, J. G. & Hulet, R. G. Realization of a measurement of a 'weak value'. *Phys. Rev. Lett.* **66**, 1107–1110 (1991).
15. Dressel, J., Malik, M., Miatto, F. M., Jordan, A. N. & Boyd, R. W. Colloquium: understanding quantum weak values: basics and applications. *Rev. Mod. Phys.* **86**, 307–316 (2014).
16. Hosten, O. & Kwiat, P. Observation of the spin Hall effect of light via weak measurements. *Science* **319**, 787–790 (2008).
17. Dixon, P. B., Starling, D. J., Jordan, A. N. & Howell, J. C. Ultrasensitive beam deflection measurement via interferometric weak value amplification. *Phys. Rev. Lett.* **102**, 173601 (2009).
18. Hallaji, M., Feizpour, A., Dmochowski, G., Sinclair, J. & Steinberg, A. M. Weak-value amplification of the nonlinear effect of a single photon. *Nat. Phys.* **13**, 540–544 (2017).
19. Weber, S. J. et al. Mapping the optimal route between two quantum states. *Nature* **511**, 570–573 (2014).
20. Murch, K. W., Weber, S. J., Macklin, C. & Siddiqi, I. Observing single quantum trajectories of a superconducting quantum bit. *Nature* **502**, 211–214 (2013).
21. Kocsis, S. et al. Observing the average trajectories of single photons in a two-slit interferometer. *Science* **332**, 1170–1173 (2011).
22. Pan, Y. et al. Weak-to-strong transition of quantum measurement in a trapped-ion system. *Nat. Phys.* **16**, 1206 (2020).
23. Kwiat, P. G. et al. High-intensity source of polarization-entangled photon pairs. *Phys. Rev. Lett.* **75**, 4337–4341 (1995).
24. Burnham, D. C. & Weinberg, D. L. Observation of simultaneity in parametric production of optical photon pairs. *Phys. Rev. Lett.* **25**, 84 (1970).
25. Li, Y. H. et al. Compact sub-GHz bandwidth single-mode time-energy entangled photon source for high-speed quantum networks. *OSA Continuum* **4**, 608–620 (2021).
26. Hanbury, B. R. & Twiss, R. Q. Correlation between photons in two coherent beams of light. *Nature* **117**, 27–29 (1956).
27. Senellart, P., Solomon, G. & White, A. High-performance semiconductor quantum-dot single-photon sources. *Nat. Nanotechnol.* **12**, 1026–1039 (2017).
28. Grangier, P., Roger, G. & Aspect, A. Experimental evidence for a photon anticorrelation effect on a beam splitter: a new light on single-photon interferences. *Europhys. Lett.* **1**, 173 (1986).
29. Bocquillon, E., Couteau, C., Razavi, M., Laflamme, R. & Weihs, G. Coherence measures for heralded single-photon sources. *Phys. Rev. A* **79**, 035801 (2009).

Methods

Hamiltonian and expressions of propagators

The Hamiltonian of single photons can be written as $H = c|\vec{p}| = c\sqrt{\hat{p}_x^2 + \hat{p}_y^2 + \hat{p}_z^2}$, where x and y are two transverse coordinates and z is the propagation direction. The momentum p_z is related to the wavelength of light, $p_z = \hbar k_z = 2\pi\hbar/\lambda$. In our experiment, the initial wave function is a Gaussian wave packet in the x–y plane, namely, $|\psi(x,y)|^2 = \mathcal{N}_G \exp[-(x^2+y^2)/(a_x^2+a_y^2)]$, where $\mathcal{N}_G$ is a normalization constant. The uncertainty of momentum p_x (p_y) is $\hbar/a_x$ ($\hbar/a_y$). The wavelength of light that we used is $\lambda = 795$ nm and $a_x = a_y \approx 0.4$ mm, so we have $p_z \gg p_x, p_y$. Under this condition, the Hamiltonian can be rewritten as an approximation

$$H \approx \frac{c\hat{p}_x^2}{2p_z} + \frac{c\hat{p}_y^2}{2p_z} + cp_z. \tag{6}$$

For the sake of simplicity and without loss of generality, we focus only on the x–z plane. In addition, because we consider p_z to be a near constant, z is proportional to the propagation time $t = z/c$. Then, the evolution of the spatial wave function $\psi(x, t)$ is described by a Schrödinger-like equation

$$i\hbar\frac{\partial}{\partial t}\psi(x,t) = \frac{c\hat{p}_x^2}{2p_z}\psi(x,t). \tag{7}$$

This result shows that the photon acts like a non-relativistic particle with effective mass $m = \frac{p_z}{c} = \frac{2\pi\hbar}{\lambda c}$ in transverse dimensions when the propagation momentum is much greater than the uncertainty of the transverse momentum[30]. As shown in Supplementary Section 7 and ref. 26, equation (7) can also be derived from the paraxial Helmholtz equation.

If we choose refractive index as a function of x, then the photons will have an effective potential $V(x)$ and act as a non-relativistic particle with a Hamiltonian $H = p_x^2/2m + V(x)$. Therefore, the propagator of single photons in free space for two fixed points (x_a, t_a) and (x_b, t_b) is given by

$$K_f(x_b, t_b; x_a, t_a) = \sqrt{\frac{m}{2\pi i\hbar t_{ba}}}\exp\left(\frac{im(x_b - x_a)^2}{2\hbar t_{ba}}\right), \tag{8}$$

where $t_{ba} = t_b - t_a$. The propagator in a harmonic potential $V(x) = m\omega^2x^2/2$ is given by[3]

$$K_h(x_b, t_b; x_a, t_a) = \mathcal{N}_h \exp\left\{\frac{im\omega}{2\hbar\sin\omega t_{ba}}\left[\left(x_a^2 + x_b^2\right)\cos\omega t_{ba} - 2x_a x_b\right]\right\}, \tag{9}$$

where $\mathcal{N}_h = \sqrt{\frac{m\omega}{2\pi i\hbar\sin\omega t_{ba}}}$.

Measurement of propagators

We take the propagator $K(x_m, t; x_a, t_a)$ with x_m being one of the points at time t as an example to describe our scheme of measuring propagators. We first divide the transverse position into d slits, so a wave function of transverse position at time t can be written as $|\psi(t)\rangle = \sum_{j=1}^{d}\psi(x_j, t)|x_j\rangle$ in basis $|x\rangle$. We choose a two-dimensional qubit space with eigenstates $|0\rangle$ and $|1\rangle$ as the pointers. Our initial state $|\phi_i\rangle$ at t_a is prepared as

$$|\phi_i\rangle = |\psi\rangle|0\rangle. \tag{10}$$

At this moment, we perform an interaction[31] $H_I = \hat{\pi}_{x_a}\hat{\sigma}_y$ with $\hat{\pi}_{x_a} = |x_a\rangle\langle x_a|$ on the system, and we have

$$U(\theta)|\phi_i\rangle = e^{-i\theta\hat{\pi}_{x_a}\hat{\sigma}_y}|\psi\rangle|0\rangle, \tag{11}$$

where θ is an angle related to the interaction strength. It also reflects whether a measurement is strong or weak. In our case, we choose a strong interaction with $\theta = \pi/2$. After this, the system state is given by

$$|\phi_a\rangle = [|\psi\rangle - \psi(x_a, t_a)|x_a\rangle]|0\rangle - \psi(x_a, t_a)|x_a\rangle|1\rangle. \tag{12}$$

Then, the system evolves with a Hamiltonian $H = p_x^2/2m + V(x,t)$ till time t, and we have an evolution operator $\hat{T}(t - t_a) = \exp[-(i/\hbar)\int_{t_a}^{t} H dt']$. The state becomes

$$\begin{aligned}|\phi_t\rangle = {} & [\hat{T}(t-t_a)|\psi\rangle - \psi(x_a,t_a)\hat{T}(t-t_a)|x_a\rangle]|0\rangle \\ & -\psi(x_a,t_a)\hat{T}(t-t_a)|x_a\rangle|1\rangle.\end{aligned} \tag{13}$$

At time t, we perform a post-selection by projecting the system to a position state $\langle x_m|$. The final state of the pointer $|f\rangle = \langle x_m|\phi_t\rangle$ can be written as

$$\begin{aligned}|f\rangle = {} & \left[\langle x_m|\hat{T}(t-t_a)|\psi\rangle\right. \\ & \left.-\psi(x_a,t_a)\langle x_m|\hat{T}(t-t_a)|x_a\rangle\right]|0\rangle \\ & -\psi(x_a,t_a)\langle x_m|\hat{T}(t-t_a)|x_a\rangle|1\rangle.\end{aligned} \tag{14}$$

Since the propagator $K(x_m, t; x_a, t_a) = \langle x_m|\hat{T}(t - t_a)|x_a\rangle$, it can be rewritten as

$$\begin{aligned}|f\rangle = {} & [\psi(x_m,t) - \psi(x_a,t_a)K(x_m,t;x_a,t_a)]|0\rangle \\ & -\psi(x_a,t_a)K(x_m,t;x_a,t_a)|1\rangle.\end{aligned} \tag{15}$$

Here, we notice that the information of propagator $K(x_b, t_b; x_a, t_a)$ is contained in the pointer. The method of extracting the propagator is similar to that of extracting the wave function in the 'direct measurement' scheme developed in another work[4]. If we measure the expectation value of the operators $\hat{\sigma}_x$, $\hat{\sigma}_y$ and $\hat{P}_1 = |1\rangle\langle 1|$, we have

$$\begin{aligned}\langle f|\hat{\sigma}^-|f\rangle = {} & -\psi^*(x_m,t)\psi(x_a,t_a)K(x_m,t;x_a,t_a) \\ & +|\psi(x_a,t_a)K(x_m,t;x_a,t_a)|^2, \\ \langle f|\hat{P}_1|f\rangle = {} & |\psi(x_a,t_a)K(x_m,t;x_a,t_a)|^2,\end{aligned} \tag{16}$$

where $\hat{\sigma}^- = \frac{1}{2}(\hat{\sigma}_x - i\hat{\sigma}_y)$. Finally, the propagator can be obtained as

$$K(x_m,t;x_a,t_a) = \frac{K'(x_m,t;,x_a,t_a)}{\psi^*(x_m,t)\psi(x_a,t_a)}, \tag{17}$$

where $K'(x_m,t;,x_a,t_a) = \frac{1}{2}[-\langle f|\hat{\sigma}_x|f\rangle + i\langle f|\hat{\sigma}_y|f\rangle] + \langle f|\hat{P}_1|f\rangle$. The wave functions $\psi^*(x_m, t)$ and $\psi(x_a, t_a)$ can be measured using the 'direct measurement' method described in previous works[4,9,11,26] and Supplementary Section 1.

However, it is difficult to extract the propagator using equation (17) when $\psi(x_m, t) \approx 0$. To solve this problem, we propose an optimized scheme. We separate the system into two branches at t_a. These two branches evolve differently and can be written as

$$\begin{aligned}|\phi_1\rangle = {} & [\hat{T}_1(t-t_a)|\psi\rangle - \psi(x_a,t_a)\hat{T}_1(t-t_a)|x_a\rangle]|0\rangle \\ & -\psi(x_a,t_a)\hat{T}_1(t-t_a)|x_a\rangle|1\rangle, \\ |\phi_2\rangle = {} & [\hat{T}_2(t-t_a)|\psi\rangle - \psi(x_a,t_a)\hat{T}_2(t-t_a)|x_a\rangle]|0\rangle \\ & -\psi(x_a,t_a)\hat{T}_2(t-t_a)|x_a\rangle|1\rangle.\end{aligned} \tag{18}$$

We choose $\hat{T}_1(t - t_a) = e^{-\frac{i}{\hbar}\int_{t_a}^{t}[\frac{p^2}{2m} + V(x,t')]dt'}$ as the evolution related to the measured propagator. In other words, $|\phi_1\rangle$ is the probe branch, which will yield the propagator $K(x_m, t; x_a, t_a) = \langle x_m|\hat{T}_1(t - t_a)|x_a\rangle$. Also, $|\phi_2\rangle$ is a reference branch, which we set to be a purely free evolution $\hat{T}_2(t - t_a) = e^{-\frac{i}{\hbar}\int_{t_a}^{t}\frac{p^2}{2m}dt'}$. We rotate $|\phi_2\rangle$ with a unitary operator, $e^{i\frac{\pi}{4}\hat{\sigma}_y}|\phi_2\rangle$. We then perform the projection operator of state $|1\rangle$ on $|\phi_1\rangle$ and perform the projection operator of state $|0\rangle$ on $e^{i\frac{\pi}{4}\hat{\sigma}_y}|\phi_2\rangle$. The results can be written as

$$\begin{aligned}|\phi_1'\rangle &= |1\rangle\langle 1|\phi_1\rangle \\ &= -\psi(x_a,t_a)\hat{T}_1(t-t_a)|x_a\rangle|1\rangle, \\ |\phi_2'\rangle &= |0\rangle\langle 0|e^{i\frac{\pi}{4}\hat{\sigma}_y}|\phi_2\rangle \\ &= \frac{1}{\sqrt{2}}\hat{T}_2(t-t_a)|\psi(x_a,t_a)\rangle|0\rangle.\end{aligned} \tag{19}$$

After that, we merge the two branches as

$$\begin{aligned}|\phi'\rangle &= |\phi_1'\rangle + |\phi_2'\rangle \\ &= \frac{1}{\sqrt{2}}\hat{T}_2(t-t_a)|\psi\rangle|0\rangle \\ &\quad -\psi(x_a,t_a)\hat{T}_1(t-t_a)|x_a\rangle|1\rangle.\end{aligned} \tag{20}$$

Then, we project $|\phi'\rangle$ on the post-selected position state $\langle x_m|$, and the result is given by

$$\begin{aligned}|f'\rangle &= \langle x_m|\phi'\rangle \\ &= \frac{1}{\sqrt{2}}\langle x_m|\hat{T}_2(t-t_a)|\psi\rangle|0\rangle \\ &\quad -\psi(x_a,t_a)K(x_m,t;x_a,t_a)|1\rangle.\end{aligned} \tag{21}$$

If the free evolution $\hat{T}_2(t-t_a)|\psi\rangle$ is virtually stationary, we can obtain an approximate result that $\langle x_m|\hat{T}_2(t-t_a)|\psi\rangle \approx \psi(x_m,t_a)$. We have checked this approximation and found that it is well satisfied in our experiments. Finally, the propagator $K(x_m,t;x_a,t_a)$ can be obtained as

$$K(x_m,t;x_a,t_a) = -\frac{K''(x_m,t;x_a,t_a)}{\sqrt{2}\psi^*(x_m,t_a)\psi(x_a,t_a)}. \tag{22}$$

where $K''(x_m,t;x_a,t_a) = -\langle f'|\hat{\sigma}_x|f'\rangle + i\langle f'|\hat{\sigma}_y|f'\rangle$. In this result, instead of measuring both $\psi(x_m,t)$ and $\psi(x_a,t_a)$, we just need to measure the wave functions at t_a, which do not vanish in our experimental conditions. We adopt this method in our experiments.

Phase modulation of SLM

SLM1 can perform a phase shift at a specific position. Because SLM1 uses liquid crystals for phase modulation, it can shift the light phase along an axis. In our case, the modulation axis is in the horizontal direction. We first use an HWP to rotate light from horizontal polarization $|0\rangle$ to diagonal polarization $|+\rangle = \frac{1}{\sqrt{2}}(|0\rangle + |1\rangle)$. Then, SLM1 performs a π phase shift on $|0\rangle$ ($|H\rangle$) at position x. The polarization after this modulation can be written as $\frac{1}{\sqrt{2}}(e^{i\pi}|0\rangle + |1\rangle) = \frac{1}{\sqrt{2}}(-|0\rangle + |1\rangle) = -|-\rangle$, which is equivalent to the operator $U = e^{-i\frac{\pi}{2}\hat{\pi}_x\hat{\sigma}_y}$. The reflected lights from SLM1 pass the HWP again. The HWP performs a reverse transformation that rotates $|-\rangle$ to $|1\rangle$ and $|+\rangle$ to $|0\rangle$.

The phase modulation of SLM1 may lead to a fluctuation described by $e^{i\epsilon\hat{\sigma}_y}$ with ϵ being a small angle, which corresponds to the background grey level displayed on SLM1. To eliminate this error, we have measured this background and deducted it from the measurement of $\langle f|\hat{\sigma}_x|f\rangle$ and $\langle f|\hat{\sigma}_y|f\rangle$.

Global phase factor of propagators

Shifting an arbitrary global phase to the propagator K will not change the physical observations. Therefore, to clearly compare the theoretical and observed propagators in Figs. 3 and 4, we have shifted a global phase $e^{i(\beta_m-\beta_t)}$ on the theoretical propagator. Here, the phase angles $\beta_m = \arctan\left(\frac{\mathrm{Re}[K_m]}{\mathrm{Im}[K_m]}\right)$ and $\beta_t = \arctan\left(\frac{\mathrm{Re}[K_t]}{\mathrm{Im}[K_t]}\right)$, where the measured (theoretical) propagator is denoted as K_m (K_t).

Calculations of classical trajectories with PLA

Here, we show that the wave functions do not have to be measured to calculate the classical trajectories with experimental data. From equation (17), we have $K'(x_b,t_b;x,t) = \psi^*(x_b,t_b)\psi(x,t)K(x_b,t_b;x,t)$, where $K(x_b,t_b;x,t) = \mathcal{N}_b\exp(\frac{i}{\hbar}S_b(x))$, and $K'(x,t;x_a,t_a) = \psi^*(x,t)\psi(x_a,t_a)K(x,t;x_a,t_a)$, where $K(x,t;x_a,t_a) = \mathcal{N}_b\exp(\frac{i}{\hbar}S_a(x))$. Here, $\mathcal{N}_a$ and $\mathcal{N}_b$ are normalization constants and are independent of x (for example, equations (8) and (9)). Therefore, we obtain

$$\Pi(x,t) = \frac{\Pi'(x,t)}{\psi^*(x_b,t_b)\psi(x_a,t_a)|\psi(x,t)|^2} = \frac{\mathcal{M}'(x,t)}{F(\gamma)}, \tag{23}$$

where $\mathcal{M}'(x,t) = \Pi'(x,t)/|\Pi'(x,t)|$ with $\Pi'(x,t) = K'(x_b,t_b;x,t)K'(x,t;x_a,t_a)$. Here, $F(\gamma) = e^{i\gamma}/\mathcal{N}^2$ with $e^{i\gamma} = \frac{\psi(x_a,t_a)\psi^*(x_b,t_b)}{|\psi(x_a,t_a)\psi^*(x_b,t_b)|}$ being an x-independent function. Similarly, from equation (22), we may obtain $\Pi(x,t) = \mathcal{M}''(x,t)/F(\gamma'')$, where $\mathcal{M}''(x,t) = \Pi''(x,t)/|\Pi''(x,t)|$ with $\Pi''(x,t) = K''(x_b,t_b;x,t)K''(x,t;x_a,t_a)$ and $e^{i\gamma''} = \frac{\psi(x_a,t_a)\psi^*(x_b,t_a)}{|\psi(x_a,t_a)\psi^*(x_b,t_a)|}$. Therefore, although the measurement of the wave function is required for the detection of propagators, it is not needed in calculating the extremum of $\Pi(x,t)$. Derived from equation (2), the PLA can be expressed as

$$\frac{\partial}{\partial x}\mathrm{Re}[\Pi(x,t)] = 0, \quad \frac{\partial}{\partial x}\mathrm{Im}[\Pi(x,t)] = 0. \tag{24}$$

Equation (5) can be derived from equation (24).

GRIN lens

In our experiment, a GRIN lens is used to form a harmonic potential for photons. The refractive index of the GRIN lens can be expressed as

$$n(r) = n_0\left(1 - \frac{1}{2}Ar^2\right), \tag{25}$$

where $n_0 = 1.643$ is the maximum refractive index of the sample, $r = \sqrt{x^2+y^2}$ and $A = 0.043\ \mathrm{mm}^{-2}$ is the gradient constant. The effective potential for the photons is a harmonic potential $V(r) = \frac{1}{2}m\omega^2r^2$, where $\omega = 2\pi/T$ with $T = 30.26\ \mathrm{mm}\ c^{-1}$ being the length of one cycle of light travel in the GRIN lens. With the constraint on one dimension $y = 0$, we have $V(x) = \frac{1}{2}m\omega^2x^2$.

Robustness of classical trajectories

In our experiment, the fluctuations of some experimental parameters, such as the control time and the relative distance between optical elements, can affect the measurement of the propagators, but classical trajectories calculated with the PLA are very robust. Here, we take the uncertainty of control time as an example. We calculate the ideal $\mathcal{M}''(x,t)$ and a deviation of the propagator $\mathcal{M}_\epsilon''(x,t) = \frac{K''(x_b,t_b;x,t)K''(x,t-\epsilon;x_a,t_a)}{|K''(x_b,t_b;x,t)K''(x,t-\epsilon;x_a,t_a)|}$ induced by a small deviation of time $\epsilon = 0.003(t_b - t_a)$. The comparison is plotted in Fig. 5. It shows that the deviation of $\mathcal{M}''(x,t)$ for a very small change in intermediate time t is small near the classical position but large in regions far away from the classical position. The fidelity of the measured propagators is given by $F = |\int_{-L/2}^{L/2}[\mathcal{M}''(x,t)]^*\mathcal{M}_\epsilon''(x,t)\mathrm{d}x|^2 = 0.6853$, where L is the measuring range of x. The difference between the classical positions calculated from $\mathcal{M}''(x,t)$ and $\mathcal{M}_\epsilon''(x,t)$ is smaller than $10^{-3}L$. Thus, the classical trajectories calculated with the PLA based on experimental data are very robust against perturbations, whereas the fidelity of the measured $\mathcal{M}''(x,t)$ is strongly affected.

Data availability

The data supporting the results of this study are available within the Article and its Supplementary Information. The raw datasets generated during the study are too large to be publicly shared, but they are available from the corresponding authors upon reasonable request.

References

30. Wen, Y. L., Zhang, S. C., Yan, H. & Zhu, S. L. Increasing the efficiency of post-selection in direct measurement of the quantum wave function. *Chinese Phys. B* **31**, 034206 (2022).

31. von Neumann, J. *Mathematical Foundations of Quantum Mechanics* (Princeton Univ. Press, 1955).

Acknowledgements

We thank Z. Y. Zhou for helpful discussions. This work was supported by the Key Area Research and Development Program of Guangdong Province (grant nos. 2019B030330001 (S.-L.Z. and H.Y.) and 2020A1515110848 (S.Z.)), the National Key Research and Development Program of China (grant nos. 2020YFA0309500 (S.Z.) and 2022YFA1405300 (S.-L.Z.)), the National Natural Science Foundation of China (grant nos. 12225405 (H.Y.), 12004120 (Y.W.), 62005082 (J.L.), 12074180 (S.-L.Z.) and U20A2074 (H.Y.)) and the Innovation Program for Quantum Science and Technology (grant no. 2021ZD0301705 (H.Y. and S.-L.Z.)).

Author contributions

Y.-L.W. and S.-L.Z. developed the theory. Y.-L.W., Y.W., S.Z., H.Y. and S.-L.Z. designed the experiment. Y.-L.W., Y.W., L.-M.T., S.Z., J.L. and J.-S.D. carried out the experiments. Y.-L.W., Y.W., H.Y. and S.-L.Z. conducted the raw data analysis. Y.-L.W., H.Y. and S.-L.Z. wrote the paper, and all authors discussed the content of the paper. H.Y. and S.-L.Z. supervised the project.

Competing interests

The authors declare no competing interests.

Additional information

Supplementary information The online version contains supplementary material available at https://doi.org/10.1038/s41566-023-01212-1.

Correspondence and requests for materials should be addressed to Hui Yan or Shi-Liang Zhu.

Peer review information *Nature Photonics* thanks the anonymous reviewers for their contribution to the peer review of this work.